J. Bangladesh Acad. Sci. 50(2); 269–281: June 2026 DOI: https://doi.org/10.3329/jbas.v50i2.90658

Journal of Bangladesh Academy of Sciences

Journal homepage: http://www.bas.org.bd/publications/jbas.html

Research Article

Electrochemical profiling of azobenzene in cetyltrimethylammonium bromide-based organized media: Insights into interfacial dynamics

Sabikun Naher Sumi and Md. Abu Bin Hasan Susan[1*]

Department of Chemistry, University of Dhaka, Dhaka 1000, Bangladesh

ARTICLE INFO

Article History

Received: 01 March 2026

Revised: 10 May 2026

Accepted: 14 May 2026

Keywords: Azobenzene, Cetyltrimethylammonium bromide, Microemulsions, Stimuli-responsive materials, Photoelectroresponsive systems, Cyclic voltammetry.

ABSTRACT

Azobenzene (AB) and its derivatives exhibit reversible photoisomerization, making them promising candidates for molecular switches and optoelectronic applications. In this study, the electrochemical behavior of AB was investigated in surfactant-based organized media, including micelles, reverse micelles, and microemulsions formed using the cationic surfactant cetyltrimethylammonium bromide (CTAB). UV-visible spectroscopy confirmed the characteristic π-π^* electronic transition of AB, while dynamic light scattering measurements revealed nanoscale organization with particle sizes below 10 nm in all media. Cyclic voltammetry showed that the redox behavior of AB is strongly governed by the interfacial environment of the surfactant assemblies. CTAB exhibits characteristic peaks arising from the adsorption/reduction of CTA^+ at the electrode surface, which overlap with the electrochemical response of AB in micellar media. In contrast, reverse micellar and microemulsion systems exhibit well-defined cathodic (~ -0.70 V) and anodic (~ 0.25 V) peaks of AB with the interference of CTAB reduction. The results highlight the influence of surfactant-based nanostructures on the electrochemical properties of AB, with a foundation for designing photoresponsive molecular devices with enhanced electrochemical control.

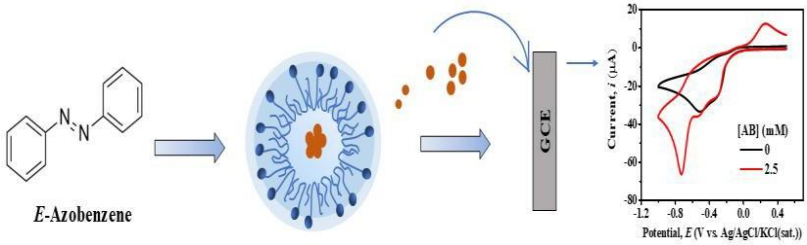

Introduction

Stimuli-responsive materials can alter their intrinsic chemical or physical properties reversibly in response to external stimuli, such as light, temperature, electric fields, magnetic fields, and pH variations (Liu et al., 2017; Stuart et al., 2010). These interactive, adaptive, and self-regulating features make them attractive materials for smart and multifunctional sensors in various domains of research, including drug delivery, biosensing, smart coatings, self-healing materials, actuators, and artificial muscles (Ceamanos et al., 2020; Kehe et al., 2019; Municoy et al., 2020; Zhang et al., 2021). Multifunctional systems that combine several stimulus responses on a single material

*Corresponding author:<susan@du.ac.bd>

[1]*Dhaka University Nanotechnology Center (DUNC), University of Dhaka, Dhaka 1000, Bangladesh*

platform have advanced significantly in recent years, allowing greater control over structure-property interactions (Campos et al., 2024; Cao et al., 2024; Whitmire, 2018).

Light is particularly attractive among various stimuli because it enables remote, non-invasive, and spatiotemporally precise control of material behavior. As a result, photoresponsive materials have become a prominent class of smart materials (Liao and Wang, 2024; Yadav et al., 2016). Their strong and reversible photoisomerization behavior has made aromatic azo compounds, azobenzene (AB) and its derivatives, prototype systems. AB undergoes reversible *E-Z* isomerization upon ultraviolet or visible light irradiation. This is accompanied by significant changes in molecular geometry, polarity, and electronic structure (Khan, 2024; Mahimwalla et al., 2012). This photoisomerization makes AB an ideal molecular switch for a wide range of applications, including drug delivery, molecular electronics, optical data storage, smart polymers, and photonic devices (Gindre et al., 2006; Kim et al., 2011; Zhu et al., 2022). Photo-induced isomerization can also be coupled with electrochemical processes, enabling control over redox behavior, charge transfer, and conductivity, thereby making the compounds dually responsive.

The electrochemical behavior of AB has been extensively investigated in non-aqueous solvents, where its reduction proceeds via two sequential one-electron transfer steps. The first step is a reversible reduction to radical monoanion, and the second is the irreversible formation of stable dianion (Bellamy et al., 1983). However, in protic or aqueous solution, AB follows different electrochemical pathways; it is reduced in a single 2-electron step to hydrazobenzene, involving proton-coupled electron transfer (PCET) mechanisms (Huang and Lessard, 2016). These observations show the critical role of the solvent environment, proton availability, and local microenvironment in controlling the redox behavior of AB. AB and their derivatives need to be solubilized in a suitable solvent to incorporate them in photoelectrochromic devices, which support both ion conduction and long-term chemical stability. Non-aqueous solvents commonly used in electrochemical studies suffer from limitations such as toxicity, volatility, high cost, and limited environmental compatibility (Darling et al., 2014). Moreover, solubilization strongly influences the photoisomerization efficiency and electrochemical response of AB, necessitating alternative media that offer controlled microenvironments.

Surfactant-based organized media such as micelles, reverse micelles, and microemulsions offer an attractive alternative to overcome these limitations. Through spontaneous association of molecules by noncovalent interaction, supramolecular self-assemblies produce stable and well-defined structures capable of solubilizing hydrophobic molecules in aqueous systems under a dynamic equilibrium (Haque et al., 2011). Incorporating an electroactive group in the structure of amphiphilic molecules has so far been the most fascinating means of exploiting the concept of self-assembly for the development of electrochemically switchable supramolecular devices (Keya et al., 2014). The presence of polarity gradients, interfacial charge distributions, and confined microenvironments within organized media significantly influences molecular orientation, diffusion, and electron-transfer kinetics (Gudla et al., 2020; Gu et al., 2025). Recent studies have demonstrated that such interfacial and confinement effects play a decisive role in tuning both photochemical and electrochemical processes of guest molecules (Baby et al., 2023; Goulet-Hanssens et al., 2017; Xie et al., 2007). While the photochemical behavior of AB in surfactant assemblies has gained attention, comparative electrochemical studies across different organized media remain scarce. In particular, the role of interfacial dynamics and solubilization state on the redox response of AB has not been systematically explored. Addressing this

gap is essential for designing organized media-based photoelectroresponsive systems.

In this work, the electrochemical behavior of AB in a homogeneous aprotic medium was studied using cyclic voltammetry. Measurements were carried out in both acetonitrile (ACN) and *N*, *N*-dimethylformamide (DMF), as aprotic solvents. ACN and DMF are employed for their high dielectric constants, good solvation ability for AB, and wide electrochemical potential windows. Both tetrabutylammonium perchlorate (TBAP) and tetrabutylammonium hexafluorophosphate ($TBAPF_6$) were used as supporting electrolytes in ACN, whereas only $TBAPF_6$ was used in DMF. These electrolytes were employed to ensure electrochemical stability and minimize background interference. Tetrabutylammonium cation increases ionic mobility and reduces interactions with redox-active species because it has weak ion-pairing tendencies. (Mann, 1969). Thus, solvent polarity and electrolyte composition influence the redox response of AB and establish a reliable reference for its intrinsic electrochemical behavior. The investigation was then extended to CTAB-based organized systems, including micelles, reverse micelles, and microemulsions. CTAB, as a cationic surfactant, forms well-defined micelles with a positively charged interface, enabling strong electrostatic interactions with AB and greater control over probe localization, interfacial electron transfer, and stabilization of redox intermediates compared to nonionic or anionic systems (Liu et al., 2007). Although CTAB influences the electrochemical response, this system enables fundamental insight into molecular-level interactions and their influence on the electrochemical behavior of AB in organized media. Changes in the voltammetric response were analyzed in relation to solubilization and aggregation phenomena, supported by dynamic light scattering (DLS) and UV-visible spectroscopic measurements. Comparing the results obtained in homogeneous and organized media helps to understand the role of supramolecular organization and interfacial interactions in modifying the redox behavior of AB, which is relevant to its performance in photoelectroresponsive materials and related applications. In such applications, surfactant-based media are employed to control molecular organization while achieving intrinsic electrochemical responses of the probe. The observed behavior in CTAB systems highlights these interfacial constraints and motivates the transition toward nonionic platforms for improved photoelectrochemical performance of AB.

Materials and Methods

Materials

Azobenzene (TCI, Tokyo, Japan), acetonitrile (Merck, Germany), *N*, *N*-dimethylformamide (Duksan, South Korea), tetrabutylammonium perchlorate (Macklin, China), tetrabutylammonium hexafluorophosphate (Wako, Japan), and potassium chloride (Sigma-Aldrich, USA) were used as received. Cetyltrimethylammonium bromide was used as the cationic surfactant, cyclohexane as the oil phase, and 1-butanol as the co-surfactant of microemulsion, all obtained from Merck and used without further purification.

Preparation of Solutions

Preparation of Non-aqueous AB Solution in Organic Solvent

Due to the low solubility of AB in water (6.4 mg/L at 25 °C), AB solutions were prepared in ACN and DMF. Stock solutions of the supporting electrolytes TBAP and $TBAPF_6$ were first prepared in the chosen organic solvent, and AB was then dissolved in these stock electrolyte solutions by appropriate dilution to yield working solutions with varying AB concentrations at a constant electrolyte concentration.

Preparation of AB in Aqueous Micellar Solution

Aqueous solutions were prepared by dissolving the required solid substances in de-ionized water (conductivity: 0.055 μS cm^{-1} at 25.0 °C) obtained from HPLC-grade water purification systems (BOECO, Germany). The critical micelle concentration (CMC) of CTAB is approximately 0.9

mM at 25 °C. A stock micellar CTAB solution of 0.03 M was prepared by dissolving 0.547 g of CTAB in 50.0 mL of de-ionized water in a volumetric flask. Solutions of varying concentrations (0.01 M and 0.02 M) were prepared by diluting the stock solution. The stock solution of approximately

0.05 mM AB was prepared by dissolving 0.5 mg AB directly into the micellar CTAB stock solution. All experiments were conducted at 25.0 ± 0.5 °C.

Preparation of Reverse Micelles and Microemulsions

By varying the proportions of water and 1-BuOH, reverse micelles of the CTAB/1-BuOH/H_2O were prepared at 20.0 % weight of CTAB (Valiente and Rodenas, 1993). Table 1 shows the compositions of reverse micelles.

Table 1. Compositions of reverse micelles.

Reverse Micelle	CTAB (% wt)	1-BuOH (% wt)	H2O (% wt)	Water to surfactant molar ratio, W_0
RM-7		7.0	73.0	73.7
RM-17	20.0	17.0	63.0	63.7
RM-27		27.0	53.0	53.5

CTAB/cyclohexane/1-BuOH/H2O microemulsions were prepared, keeping the CTAB/cyclohexane ratio fixed with varying proportions of 1-BuOH and H_2O, ranging from high H_2O to 1-BuOH content. Various compositions of microemulsions are shown in Table 2.

Table 2. Compositions of microemulsions

Microemul-sion	CTAB (%wt)	Cycloh-exane (% wt)	1-BuOH (%wt)	H_2O (% wt)	W_0
ME-17			17.0	59.6	60.3
ME-27	20.0	3.4	27.0	49.6	50.2
ME-37			37.0	39.6	40.1

Reverse micelles and microemulsions were designated according to the weight percentage of 1-BuOH. Required concentrations of AB were prepared by dissolving weighed amounts in different compositions of reverse micelles and microemulsions.

Electrochemical Measurements

A computer-controlled electrochemical analyzer (CHI 650D, CH Instruments, USA) was employed for the cyclic voltammetric measurements. For aqueous solutions, an Ag/AgCl/KCl (sat.) reference electrode was employed, whereas an $Ag/AgNO_3$ reference electrode was employed for non-aqueous solutions. Electrochemical measurements were performed using a glassy carbon electrode (GCE) with a geometric area of 0.071 cm^2 as the working electrode and a Pt-wire as a counter electrode in a single-compartment cell. Before each run, the surface of the GCE was polished with alumina powder (0.30 µm and 0.05 µm), received from Buehler.

The electrochemical measurements of AB in ACN were carried out in the presence of TBAP as a supporting electrolyte, while in aqueous micellar solution, the measurements were carried out using 0.025 M KCl as the supporting electrolyte. Before the electrochemical experiments, the surfactant solutions were purged with N_2, and this inert atmosphere was kept throughout the course of the experiments. The potential sweep rate (v) was between 10 and 500 mV s^{-1}.

Spectrophotometric Measurements

A double-beam UV-visible spectrophotometer (Shimadzu UV Spectrophotometer, UV-1800) was employed to obtain the absorption spectra of AB in non-aqueous and aqueous micellar solutions. Throughout the investigation, rectangular quartz cells with a path length of 1.0 cm were used.

Particle Size Measurements

The hydrodynamic diameter of the CTAB-based organized media was measured using a Zetasizer Nano ZS90 (ZEN3690, Malvern Instruments Ltd, UK) equipped with a Peltier temperature control. A He-Ne laser operating at 632.8 nm in wavelength was

employed as the light source in the experiments. The scattering angle was fixed at 90°. A 10 mm glass cuvette was used as the sample cell. Before each measurement, the cell was washed carefully with de-ionized water and ethanol to avoid any contamination and ensure optical transparency. At each temperature, three measurements were performed, each consisting of 20 runs with a 20-second runtime.

Results and Discussion

AB in Non-aqueous Solutions

UV-visible absorption spectra were recorded for 0.05 mM AB in ACN (Fig. 1 (a)). The spectrum shows that AB exhibits π-π* transition at ~ 306 nm, whereas n-π* transition at ~ 440 nm, which is consistent with literature values (300-330 nm and 420-450 nm, respectively) for *E*-AB. Cyclic voltammetric measurements of AB at a GCE against the $Ag/AgNO_3$ reference electrode in ACN containing 0.10 M TBAP as the supporting electrolyte were conducted at different scan rates. The cyclic voltammograms (CV) of AB are displayed in Fig. 1 (b-d). Two cathodic features are observed during the cathodic sweep from 0 V to -2.0 V. The first cathodic response (~ -1.2 V) and its corresponding anodic feature arise from background processes associated with the supporting electrolyte and the electrode electrolyte interface. In contrast, the second cathodic peak (~ -1.75 V) is attributed to the electrochemical reduction of AB. AB exhibits an apparent one-step, two-electron reduction, where two closely spaced electron-transfer steps merge into a single cathodic peak due to the short-lived nature of the intermediate radical anion, as reported for azo compounds in aprotic media (Bellamy et al., 1983). The anodic peak observed during the reverse scan corresponds to the oxidation of the reduced AB species. The perchlorate anion, owing to its relatively weak coordinating ability and higher polarizability, facilitates better stabilization of the electrochemically generated radical anion of AB, thereby enhancing electron-transfer kinetics and current response. As the concentration of AB increases (Fig. 1 (c)), its local concentration near the electrode surface also increases, thus the current also increases.

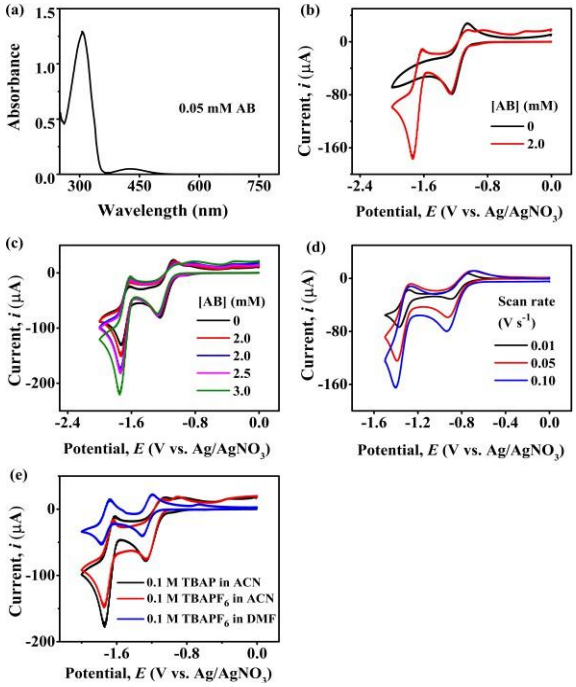

Fig. 1. (a) UV-visible absorption spectra of 0.05 mM AB in ACN, (b) CVs in the presence and absence of 2.0 mM AB, (c) varying concentration of AB at a scan rate of 0.10 V s^{-1}, (d) 2.0 mM AB in ACN/TBAP (0.10 M) at varying scan rates, and (e) at 2.0 mM AB in various non-aqueous media, varying solvent and electrolyte.

To investigate the scan rate dependence of the cyclic voltammetric behavior of AB in ACN, CVs recorded at varying scan rates are shown in Fig. 1 (d). The peak-to-peak separation (ΔE) exceeds the theoretical value of 59/*n* mV expected for a fully reversible Nernstian process, ranging from 90 to 150 mV. This deviation indicates a quasi-reversible process influenced by slow electron-transfer kinetics and a coupled chemical reaction. The involvement of the chemical process suppresses ideal Nernstian behavior and contributes to the quasi-reversible voltammetric responses. Logarithmic profile of peak current against scan rate is found to be linear with the best fit obtained with an acceptable regression coefficient (>0.991). The slope, a = 0.43, is close to 0.5, which indicates that the system is diffusion-

controlled, and the possibility of following chemical processes can't be neglected.

Despite being an aprotic solvent, ACN does not completely preclude proton involvement in the reduction of AB. The reduction proceeds through two sequential electron-transfer steps, forming AB^{2-}. This highly basic dianionic species rapidly abstracts a proton from ACN, generating hydrazobenzene (ABH_2) along with the cyanomethyl anion (CH_2CN^-) (Schatz et al., 2025), as shown in Scheme 1. Consequently, the electrochemical response is initially dominated by electron-transfer processes at the azo (-N=N-) group, followed by a fast solvent-mediated chemical step. The faster the rate of change in potential (i.e., the scan rate), the higher the probability that nearby species will be oxidized and reduced.

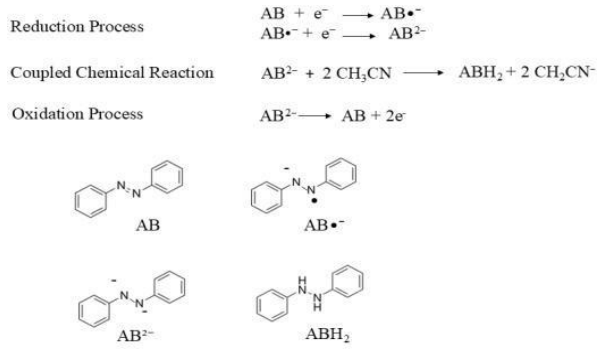

Scheme 1. Electrochemical reduction of AB in ACN via a two-electron, quasi-reversible process with solvent-mediated protonation.

In contrast, $TBAPF_6$ is used as the supporting electrolyte in ACN and DMF, and redox peaks of AB are observed in Fig. 1 (e). However, the peak currents are noticeably reduced. This behavior can be attributed to the weaker solvated and less polarizable PF_6^- anion, which leads to less effective stabilization of charged intermediates and increased ion-pairing effects, resulting in lower current response.

To investigate solvent effects on the electrochemical reduction of AB, DMF of comparable polarity with different donor ability is used (Fig. 1 (e)). Higher viscosity of DMF compared to ACN results in slower diffusion of AB, thereby decreasing the diffusion-controlled current. Stronger solvation of the supporting electrolyte ions and the reduced form of AB in DMF can hinder electron-transfer processes at the electrode-solution interface. Therefore, ACN-TBAP provides the higher current response and clearer redox features, while changes in electrolyte and solvent polarity reduce electrochemical activity.

AB in Aqueous Systems

AB in Aqueous Micellar Systems of CTAB

AB has very low solubility in aqueous media due to its hydrophobic nature, but CTAB micelles incorporate it into the hydrophobic core or palisade layer of micelles. Thus, micelles enhance the dispersion and effective solubility of AB, acting as nanocarriers. DLS measurements were carried out to determine the hydrodynamic diameter of the micellar system. Fig. 2 represents the intensity and number-based particle size distribution (PSD) of CTAB-based micelles, concentration above CMC at 0.01 M, containing 0.05 mM AB. The intensity-based size distribution shows multiple size aggregates, where larger particles dominate due to the strong size dependence of scattering intensity. In contrast, the number-based distribution indicates that the majority of particles are confined to the small size range (~1-3 nm). Therefore, the system is composed of nanoscale organizations, with larger sizes representing only a minor fraction of aggregates.

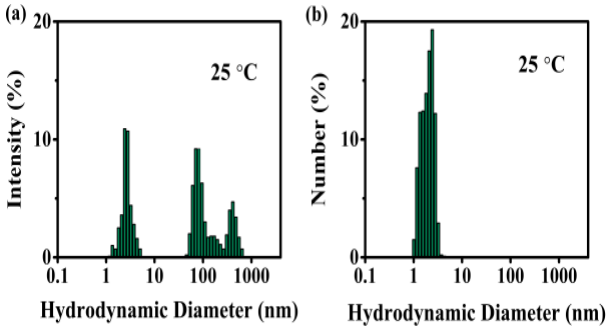

Fig. 2. (a) Intensity-based and (b) number-based PSD in the presence of 0.05 mM AB in 0.01 M CTAB-based micellar system. (Hydrodynamic diameters are plotted in logarithmic scales).

UV-visible absorption spectra were recorded for varying concentrations of AB in 0.01 M CTAB-based micellar system and 0.05 M AB in varying concentrations of CTAB (Fig. 3). The spectra revealed that AB exhibits π-π^* transition at ~ 312 nm, whereas n-π^* transition at ~ 440 nm. At fixed CTAB concentration, AB absorbance follows Beer-Lambert's law, yielding $\varepsilon \approx 27{,}100\ M^{-1}\ cm^{-1}$ at 312 nm. However, at 0.05 mM AB, higher CTAB reduces absorbance due to micelle saturation, indicating partitioning of AB into excess micelles that dilutes the effective chromophore concentration in the system.

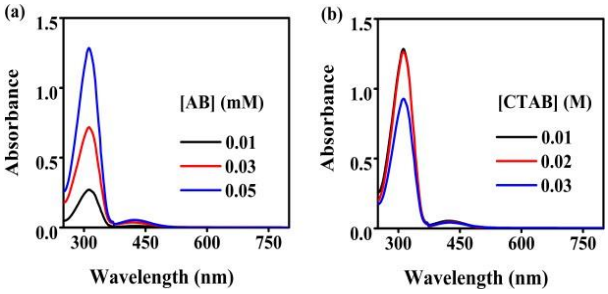

Fig. 3. UV-visible absorption spectra of CTAB-based micellar system at (a) varying concentration of AB in 0.01 M CTAB and (b) varying concentration of CTAB incorporating 0.05 mM AB.

The electrochemical behavior of AB was studied in CTAB-based micellar systems. CVs of AB were recorded at a GCE using an Ag/AgCl/KCl(sat.) reference electrode in the presence of 0.25 M KCl as the supporting electrolyte. The amphiphilic nature of CTAB directs spontaneous adsorption onto the GCE surface via electrostatic and hydrophobic interactions between CTA^+ cations and the electrode interface.

This process favors stable, micelle-like layer formation that modifies the electrode-solution interface. This adsorption appears as distinct cathodic peaks, consistent with the reported behavior (Gisbert-Gonzalez et al., 2023; Tyszczuk-Rotko and Gorylewski, 2022).

CVs recorded in both blank CTAB solutions and AB-containing micellar systems consistently exhibited two cathodic peaks across the applied potential window, with no distinct redox peaks attributable to AB reduction or oxidation (Fig. 4 (a)). The absence of AB-specific electrochemical responses suggests micellar encapsulation of hydrophobic AB restricts its diffusion to the adsorbed layer of CTAB, and the partition coefficient of AB into the micellar core rather than the electrical double layer may suppress direct electron transfer under these conditions. Therefore, CTAB adsorption and interfacial organization play a dominant role in modulating the GCE interface while indicating limited electrochemical accessibility of AB within the organized medium.

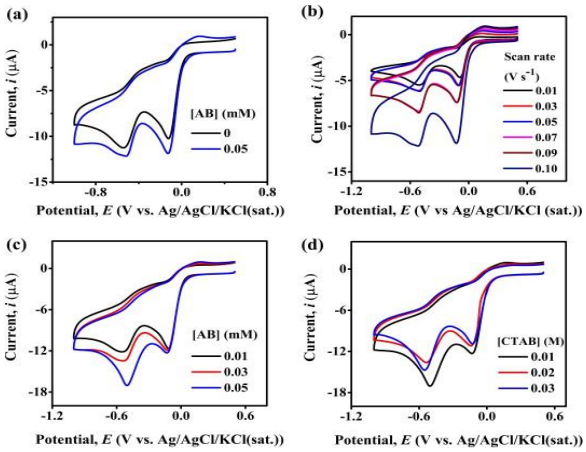

Fig. 4. CVs (a) in the presence and absence of 0.05 mM AB at scan rate 0.1 V s^{-1}, (b) at varying scan rates, (c) varying concentrations of AB in 0.01 M CTAB-based micellar system, and (d) varying concentrations of CTAB incorporating 0.05 mM AB.

CVs performed as a function of scan rate, varying AB concentration at fixed CTAB concentration (0.01 M), and varying CTAB concentration at fixed AB concentration (0.05 mM) revealed consistent voltammetric profiles (Fig. 4 (b-d)). Peak currents and integrated areas increased with increasing scan rate, indicating diffusion-controlled processes dominated by cathodic CTA^+ adsorption/reduction at the electrode interface. At constant CTAB concentration, increasing AB concentration selectively enhanced the cathodic peak to a more negative value (~ -0.5 V), leaving the less negative peak unchanged. This behavior indicates that the peak at a less negative value originates from the adsorption/reduction of CTA^+ at

the electrode interface, which is independent of AB. But the peak at a more negative value is associated with the micelle-mediated reduction of AB. Due to its hydrophobic nature, AB is solubilized in the palisade layer or hydrophobic core of CTAB micelles, requiring a higher overpotential for electron transfer.

As AB concentration increases, its local concentration within the micellar core near the electrode surface also increases, leading to enhanced current contribution at more negative potential. Conversely, at a fixed concentration of AB, increasing CTAB concentration produced minor shifts in peak potential with systematic suppression of both cathodic peak currents. This effect can be attributed to surface coverage by CTA^+ ions, competitive adsorption that blocks active sites, and dilution of AB partitioning into excess micelles. Thus, the availability of AB at the electrode surface gets reduced. The quasi-reversible nature of the CTAB processes was evident from diminished anodic peak currents relative to cathodic peaks. Thus, a primary CTAB adsorption-controlled cathodic process that is independent of AB and a secondary AB-influenced reduction pathway underscore the dominant role of surfactant organization in modulating electrochemical accessibility within the micellar assembly.

AB in Reverse Micellar Systems of CTAB

The solubility of AB in reverse micelles was markedly higher than in micelles, attributed to the hydrophobic bulk medium in reverse micelles that favors the partitioning of AB. DLS measurements confirmed the hydrodynamic diameter of the reverse micellar system incorporating AB, with both intensity- and number-based size distributions exhibiting as nanoscale organization, as shown in Fig. 5 (a-b). The intensity distribution shifted toward smaller hydrodynamic diameters with narrower peaks, with enhanced colloidal stability and uniformity compared to the broader micellar distribution. UV-visible absorption spectra were recorded for varying concentrations of AB in CTAB-based reverse micelles (RM-17) and 0.08 mM AB in varying compositions of the reverse micellar system, as shown in Fig. 5 (c-d). The spectra indicate a similar pattern to that of the micellar system. At a fixed CTAB composition, the absorbance of AB increases linearly with concentration. The CTAB concentration is kept constant while the volume of *n*-butanol increases and water content decreases, effectively altering W_0 and the reverse micellar environment. The spectra for RM-7, RM-17, and RM-27 show that the main absorption peak around ~305 nm remains relatively unchanged in wavelength, indicating that the electronic environment of AB experiences minimal polarity-induced shifts.

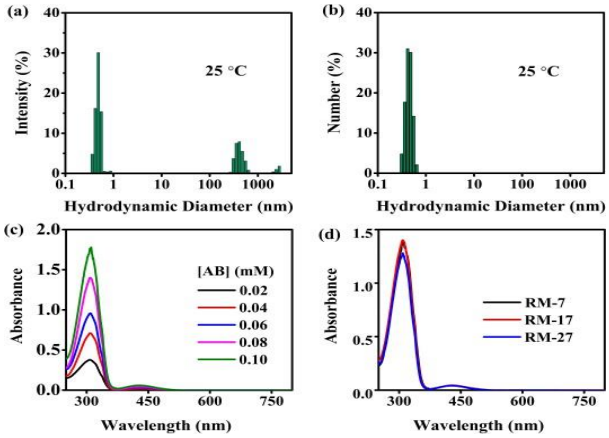

Fig. 5. (a) Intensity-based and (b) number-based PSD in the presence of 0.05 mM AB in RM-17. UV-visible absorption spectra of the CTAB-based reverse micellar system at (c) varying concentration of AB in RM-17 and (d) 0.08 mM AB in varying composition of reverse micelles.

The electrochemical behavior of AB has been studied in reverse micelles of CTAB/1-BuOH/H_2O system. Cyclic voltammetric measurements of 2.0 mM AB in reverse micelles have been carried out using 20% weight of CTAB at different compositions of water and 1-butanol without the use of any added electrolyte, as shown in Fig. 6 (a). Potential was scanned from 0.5 V to -1.0 V, followed by a reverse scan from -1.0 V to 0.5 V. A cathodic peak (-0.3 V) and its corresponding anodic peak are observed in the CV response, where AB is

absent. The observed peaks can be attributed to the redox behavior of CTAB. In the presence of AB, distinct cathodic and anodic peaks are observed at -0.64 V and 0.3 V, respectively. These peaks arise due to the redox reaction of AB. According to literature, in the protic medium, AB undergoes a single-step two-electron reduction to AB^{2-} leading to the formation of ABH_2. The electrochemical process in aqueous solution can be represented as in Scheme 2.

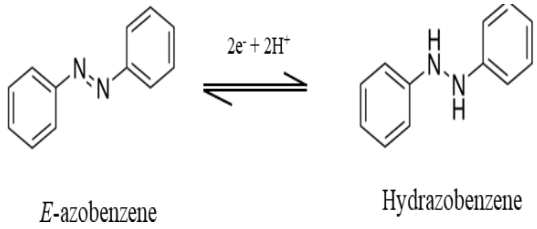

Scheme 2. Redox reaction of AB in protic media.

CVs shown in Fig. 6 (b) demonstrate the variation of concentration of AB in a fixed composition of reverse micellar system where AB is solubilized in the bulk medium. The higher the concentration of AB, the higher the number of electroactive species, and thereby the peak current increases. This is consistent with the direct relationship between peak current and concentration in diffusion-controlled electrochemical processes. Fig. 6 (c-d) shows that as the composition varies, the reduction peak of CTAB also varies. When 1-BuOH content is increased and water content is reduced in a CTAB-based reverse micellar system, smaller, more compact reverse micelles are formed. 1-BuOH as cosurfactant partially penetrates into the CTAB headgroup region. This increases interfacial fluidity and reduces reorganization energy. Consequently, electron transfer to the CTA^+ group becomes thermodynamically more favorable, and the reduction response is enhanced. The interfacial fluidity and micellar flexibility shift the electroactive species (AB) closer to the micelle-electrode interface and enhance the redox responses. Fig. 6 (e) presents the CVs of 2.0 mM AB in RM-7 recorded at different scan rates. The separation of peak potential (ΔE) is much higher than 59 mV/n (where n = 2), which indicates that the redox reaction is quasi-reversible, as the electron transfer between the electrode and the redox species is not fast enough to achieve a reversible reaction. The logarithmic profile of peak current against scan rate is linear, with a slope of 0.53, close to 0.5, indicating that the process is diffusion-controlled, with the influence of some other chemical process. The peak current observed is significantly lower than in the non-aqueous solutions, likely due to the influence of aggregation and the confined environment in the organized media.

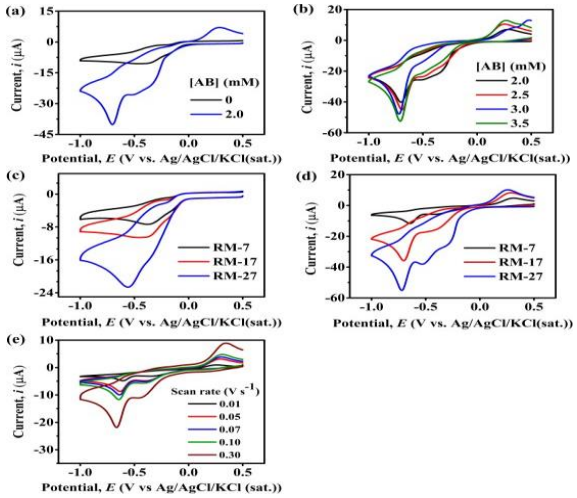

Fig. 6. CVs (a) in the presence and absence of 2.0 mM AB at scan rate 0.1 V s^{-1}, (b) varying concentrations of AB in RM-17, (c) varying composition of RM in the absence of AB, (d) 2.0 mM AB at varying composition of RM, and (e) 2.0 mM AB in RM-7 at varying scan rates.

AB in Microemulsion Systems of CTAB

The PSD analysis and UV-visible absorption studies exhibit trends consistent with those observed in the reverse micellar system. In the microemulsion system, AB is solubilized within the micellar core and confined in a hydrophobic microenvironment. Such confinement makes this system particularly favorable for studying molecular switching. The electrochemical behavior of AB was studied in CTAB/cyclohexane/1-

BuOH/H_2O microemulsion systems. CVs of AB are taken at GCE against Ag/AgCl/KCl(sat.) reference electrode. Two cathodic peaks and their corresponding anodic peaks are observed in the CV response, which is attributed to the redox behavior of CTAB. CTAB reductions are observed at -0.3 V and -0.5 V. Fig. 7. (a) shows CV of 2.5 mM AB in ME-27 at scan rate 0.1 V s^{-1}. In the presence of AB, distinct cathodic and anodic peaks are observed at -0.70 V and 0.25 V, respectively. These peaks arise due to the redox reaction of AB. AB is reduced in one step, and two electrons are transferred in the system as observed for microemulsions (*vide supra*). As the concentration of AB increases, both the anodic and cathodic currents also increase as the number of electroactive species increases (Fig. 7 (b)). This is consistent with the direct relationship between peak current and concentration in diffusion-controlled electrochemical processes. With increasing 1-butanol content and reducing water content, the microemulsion droplets undergo interfacial reorganization. The reduced water fraction diminishes hydration around the surfactant headgroups. The interfacial flexibility lowers the reorganization energy associated with the redox process, leading to enhanced electron-transfer kinetics and an increase in the observed current, as shown in Fig. 7 (c). With increasing scan rate, the current increases. The logarithmic profile of peak current against scan rate is linear, with a slope of 0.46, close to 0.5, indicating that the process is diffusion-controlled, with the influence of some other chemical process.

In this study, AB is solubilized within the cyclohexane present in the core of the microemulsion, while the surfactant forms a stable interface. When an electrochemical potential is applied, the stable interface between the oil and water phases starts to be affected, and an interplay in the reduction behavior of AB and the surfactant itself is thus observed.

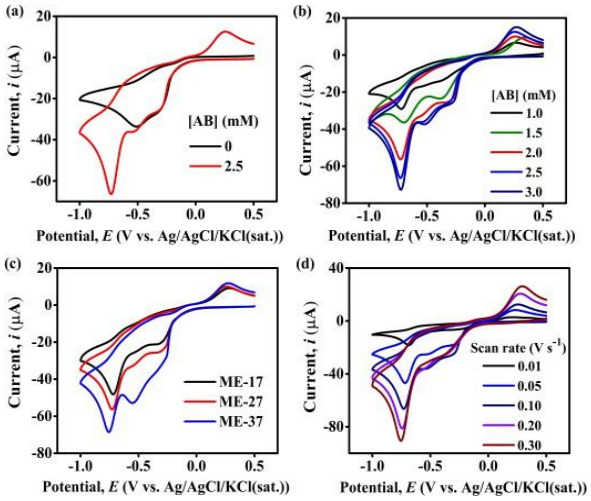

Fig. 7. CVs (a) in the presence and absence of 2.5 mM AB at scan rate 0.1 V s^{-1}, (b) varying concentrations of AB in ME-27, (c) varying composition of ME in the presence of 2.5 mM AB, (d) 2.5 mM AB in ME-27 at varying scan rates.

In the surfactant-based organized media, there exists an equilibrium between the monomeric state of CTAB and the aggregated (micellar) forms. Due to the equilibrium between the micelle and monomeric states, continuous formation and disruption of micellization occur. The interaction of AB with the two states is not similar, which also influences its electrochemical response. Also, when CTAB aggregates to form micelles, their ability to interact with the electrode surface is reduced compared to the monomeric form. The aggregation may lead to the formation of a barrier around the electrode surface, potentially inhibiting the direct contact between AB and the electrode. When the potential is applied, the aggregates diffuse to the electrode surface and disrupt into the monomeric state. AB and CTAB in the monomeric state both undergo redox reactions in the potential range. Thus, the electrochemical response of AB in microemulsion is diffusion-controlled but influenced by many other chemical processes.

Moreover, when AB is reduced to its dianion AB^{2-}, the reduced form can be further oxidized to AB or can interact with the quaternary ammonium group of

CTAB. The latter process therefore reduces the availability of AB^{2-} for electron transfer at the electrode surface, increases the separation of peak potential, and thus influences the reversibility of the redox behavior of AB. Understanding these effects is crucial for accurately interpreting the cyclic voltammograms and for optimizing the electrochemical performance of the system. A schematic representation of the electrochemical response of AB in non-aqueous solution, as well as in organized media of CTAB, is shown in Scheme 3.

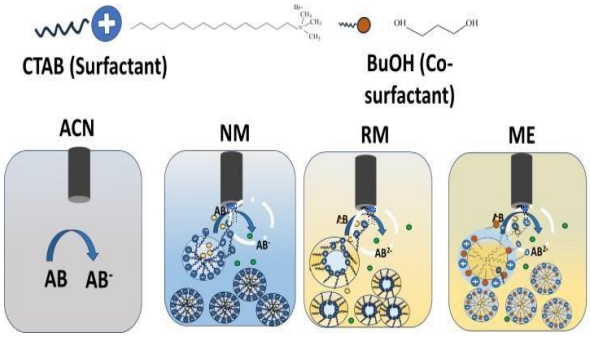

Scheme 3. Probable molecular level illustration of the reduction process in the vicinity of the electrode in three organized media- normal micelle (NM), reverse micelle (RM), and microemulsion (ME). The brown and green spheres indicate the state of AB before and after the reduction, respectively.

Conclusion

The influence of the solubilization environment on the redox behavior of azobenzene was systematically examined in CTAB-based micelles, reverse micelles, and microemulsions. AB exhibits higher solubility in reverse micelles and microemulsions than in aqueous micellar solutions. In these organized media, AB undergoes a single two-electron reduction process, while CTAB exhibits characteristic adsorption-reduction features at the electrode surface. AB shows suppressed or poorly defined redox signals in CTAB micellar systems within the studied potential window. In contrast, reverse micellar and microemulsion systems exhibit distinct, diffusion-controlled, and quasi-reversible reduction processes.

The presence of cathodic features associated with CTAB reduction indicates that the surfactant interferes with the electrochemical reversibility of AB, thereby limiting the applicability of CTAB-based organized media for molecular switching. Although AB is well solubilized in reverse micelle and microemulsion media, interactions with CTAB and co-surfactant components significantly influence its redox behavior. Future work will focus on organized media based on non-ionic or polymeric surfactants to develop AB-based photoelectrochemical switching systems.

Acknowledgment

The authors gratefully acknowledge financial support from the University Grants Commission research grant for Dhaka University teachers for a research project.

Author contribution

Sabikun Naher Sumi: Investigation, original draft, editing; Md. Abu Bin Hasan Susan: Conceptualization, supervision, review, editing, and project administration.

Conflict of interest

The author declares that there is no potential conflict of interest.

References

Baby A, Abinaya S, John AM, Jose SP, and Balakrishnan SP. Photoresponse and electrochemical behaviour of azobenzene anchored graphene oxide for energy storage application. *Mater. Chem. Phys.* 2023; 301: 127592.

Bellamy AJ, MacKirdy IS, and Niven CE. Cyclic voltammetry of azopyridines, phenylazopyridines, and azobenzene in acetonitrile and dimethylformamide. *J. Chem. Soc., Perkin Trans. 2.* 1983(2): 183–185.

Campos GC, Sáiz LM, Pettarin V, Zucchi IA, and Galante MJ. Self-healing recyclable polymers based on azobenzenes with thermoset like behaviour. *Polymer*. 2024; 290: 1–8.

Cao Y, Wu Y, Huang Y, Xiang H, and Zhang L. Photo/thermal dual-responsive azobenzene-based photosensitive resin for 4D printing. *Chem. Eng. J.* 2024; 498(21): 155140.

Ceamanos L, Kahveci Z, Lopez-Valdeolivas M, Liu D, Broer DJ, and Sánchez-Somolinos C. Four-dimensional printed liquid crystalline elastomer actuators with fast photoinduced mechanical response toward light-driven robotic functions. *ACS Appl. Mater. Interfaces.* 2020; 12(39): 44195–44204.

Darling RM, Gallagher KG, Kowalski JA, Ha S, and Brushett FR. Pathways to low-cost electrochemical energy storage: a comparison of aqueous and nonaqueous flow batteries. *Energy Environ. Sci.* 2014; 7(11): 3459–3477.

Gindre D, Boeglin A, Fort A, Mager L, and Dorkenoo KD. Rewritable optical data storage in azobenzene copolymers. *Opt. Express* 2006; 14(21): 9896–9901.

Gisbert-Gonzalez JM, Briega-Martos V, Vidal-Iglesias FJ, Cuesta A, Feliu JM, and Herrero E. Spectroelectrochemical studies of CTAB adsorbed on gold surfaces in perchloric acid. *Langmuir*. 2023; 39(7): 2761–2770.

Goulet-Hanssens A, Utecht M, Mutruc D, Titov E, Schwarz J, Grubert L, Bléger D, Saalfrank P, and Hecht S. Electrocatalytic *Z→E* isomerization of azobenzenes. *J. Am. Chem. Soc.* 2017; 139(1): 335–341.

Gu C, Liu K, Pendergast A, Kawamata Y, Baran PS, Neurock M, and Qi Y. Ion-Driven dynamics of charge-neutral species in the electrical double layer: Insights from alternating and constant polarity simulations. *ACS Electrochem*. 2025; 1(12): 2749–2760.

Gudla H, Zhang C, and Brandell D. Effects of solvent polarity on Li-ion diffusion in polymer electrolytes: An all-atom molecular dynamics study with charge scaling. *J. Phys. Chem. B.* 2020; 124(37): 8124–8131.

Haque MA, Rahman MM, and Susan MA. Aqueous electrochemistry of anthraquinone and its correlation with the dissolved states of a cationic surfactant. *J. Solution. Chem.* 2011; 40(5): 861–875.

Huang Y and Lessard J. Electrochemical behaviour of nitrobenzene, nitrosobenzene, azobenzene, and azoxybenzene on Hg, Pt, Cu, and Ni electrodes in aprotic medium. *Electroanalysis*. 2016; 28(11): 2716–2727.

Kehe GM, Mori DI, Schurr MJ, and Nair DP. Optically responsive, smart anti-bacterial coatings via the photofluidization of azobenzenes. *ACS Appl. Mater. Interfaces*. 2019; 11(2): 1760–1765.

Keya JJ, Islam MM, Rahman MM, Mollah MY, and Susan MA. Effect of a water structure modifier on the aqueous electrochemistry of supramolecular systems: Redox-active versus conventional surfactants. *J. Electroanal. Chem.* 2014; 712: 161–166.

Khan A. Cleavable azobenzene linkers for the design of stimuli-responsive materials. *Chem. Commun.* 2024; 60(52): 6591-6602.

Kim Y, Wang G, Choe M, Kim J, Lee S, Park S, Kim DY, Lee BH, and Lee T. Electronic properties associated with conformational changes in azobenzene-derivative molecular junctions. *Org. Electron.* 2011; 12(12): 2144–2150.

Liao ZH and Wang F. Light-controlled smart materials: Supramolecular regulation and applications. *Smart Mol.* 2024; 2(4): e20240036.

Liu Q, Li J, Tao W, Zhu Y, and Yao S. Comparative study on the interaction of DNA

with three different kinds of surfactants and the formation of multilayer films. *Bioelectrochem*. 2007; 70(2): 301–307.

Liu X, Yang Y, and Urban MW. Stimuli-responsive polymeric nanoparticles. *Macromol. Rapid Commun.* 2017; 38(13): 1700030.

Mahimwalla Z, Yager KG, Mamiya JI, Shishido A, Priimagi A and Barrett CJ. Azobenzene photomechanics: prospects and potential applications. *Polym. Bull.* 2012; 69(8): 967–1006.

Mann CK. Nonaqueous solvents for electrochemical use. *Electroanal. Chem*. 1969; 3: 57–134.

Municoy S, Alvarez Echazu MI, Antezana PE, Galdopórpora JM, Olivetti C, Mebert AM, Foglia ML, Tuttolomondo MV, Alvarez GS, Hardy JG, and Desimone MF. Stimuli-responsive materials for tissue engineering and drug delivery. *Int. J. Mol. Sci*. 2020; 21(13): 4724.

Schatz D and Wegner HA. Electrochemistry of azobenzenes and its potential for energy storage. *J. Org. Chem*. 2025; 90(16): 5336–5342.

Stuart MA, Huck WT, Genzer J, Müller M, Ober C, Stamm M, Sukhorukov GB, Szleifer I, Tsukruk VV, Urban M and Winnik F. Emerging applications of stimuli-responsive polymer materials. *Nat. Mater*. 2010; 9(2): 101–113.

Tyszczuk-Rotko K and Gorylewski D. Glassy carbon modified with cationic surfactant (GCE/CTAB) as electrode material for fast and simple analysis of the arsenic drug roxarsone. *Materials*. 2022; 16(1): 345.

Valiente M and Rodenas E. Influence of CTAB/alkanol/cyclohexane w/o microemulsions on the basic hydrolysis of crystal violet. *Colloid Polym. Sci*. 1993; 271(5): 494–498.

Whitmire KH. Transition metal complexes of the naked pnictide elements. *Coord. Chem. Rev*. 2018; 376: 114–195.

Xie N, Zeng DX, and Chen Y. Electrochemical switch based on the photoisomerization of a diarylethene derivative. *J. Electroanal. Chem.* 2007; 609(1): 27–30.

Yadav S, Deka SR, Verma G, Sharma AK, and Kumar P. Photoresponsive amphiphilic azobenzene–PEG self-assembles to form supramolecular nanostructures for drug delivery applications. *RSC Adv*. 2016; 6(10): 8103–8117.

Zhang Q, Zhang Y, Wan Y, Carvalho W, Hu L, and Serpe MJ. Stimuli-responsive polymers for sensing and reacting to environmental conditions. *Prog. Polym. Sci*. 2021; 116: 101386.

Zhu J, Guo T, Wang Z, and Zhao Y. Triggered azobenzene-based prodrugs and drug delivery systems. *J. Control. Release*. 2022; 345: 475–493.